UC 404
LBL-29476
Preprint

Lawrence Berkeley Laboratory
UNIVERSITY OF CALIFORNIA

Materials & Chemical Sciences Division

Submitted to Journal of the Electrochemical Society

In Situ Scanning Tunneling Microscopy of Copper Deposition with Benzotriazole

M.J. Armstrong and R.H. Muller

August 1990

For Reference

Not to be taken from this room

LBL-29476
Copy 1
Bldg. 50 Library.

Prepared for the U.S. Department of Energy under Contract Number DE-AC03-76SF00098.

DISCLAIMER

This document was prepared as an account of work sponsored by the United States Government. While this document is believed to contain correct information, neither the United States Government nor any agency thereof, nor the Regents of the University of California, nor any of their employees, makes any warranty, express or implied, or assumes any legal responsibility for the accuracy, completeness, or usefulness of any information, apparatus, product, or process disclosed, or represents that its use would not infringe privately owned rights. Reference herein to any specific commercial product, process, or service by its trade name, trademark, manufacturer, or otherwise, does not necessarily constitute or imply its endorsement, recommendation, or favoring by the United States Government or any agency thereof, or the Regents of the University of California. The views and opinions of authors expressed herein do not necessarily state or reflect those of the United States Government or any agency thereof or the Regents of the University of California.

LBL-29476

In Situ Scanning Tunneling Microscopy of Copper Deposition with Benzotriazole

Michael J. Armstrong* and Rolf H. Muller

Lawrence Berkeley Laboratory
University of California
Berkeley, CA 94720
and
Department of Chemical Engineering
University of California
Berkeley, CA 94720

This work was supported by the Director, Office of Energy Research, Office of Basic Energy Sciences, Materials Sciences Division, of the U.S. Department of Energy under Contract No. DE-AC03-76SF00098.

*Current Address: IBM Corporation, Almaden Research Center, San Jose, CA 95120-6099

In Situ Scanning Tunneling Microscopy of Copper Deposition with Benzotriazole

Abstract

The sub-micron topography of Cu deposits has been studied with scanning tunneling microscopy to investigate the effect of benzotriazole in the initial stages of deposition. The presence of benzotriazole results in a marked increase in overpotential for the deposition. It is found to eliminate the preferential growth of specific crystallographic planes and the formation of crystal facets. The number density of nuclei, determined from Fourier transforms of the surface profiles of 7 nm-thick films, is found to increase with increasing overpotential of the deposition but is dependent of the presence of the inhibitor.

Introduction

A metal surface appears bright when most of the energy of an incident light beam is specularly reflected. The brightness of a deposit is related to its microtopography.[1] A bright deposit has a characteristic roughness less than the wavelength of the incident visible light (0.4 to 0.7 μm).

Bright deposition of Cu is not usually obtained with electrolytes composed of simple salts of Cu because at high overpotentials mass-transfer limited deposition results in favored growth of protrusions and at low overpotentials the growth of large particles is favored. Organic and inorganic additives are used in Cu plating baths to increase the deposit brightness. Benzotriazole has been shown to be an effective brightening agent at concentrations greater than 100 μM in acid copper sulfate electrolyte.[2] The deposition of Cu in the presence of benzotriazole (BTA) was chosen as a model system to study the developing topography of bright deposits.

The addition of 100 μM BTA to a 0.05M $CuSO_4$ solution has been shown to increase the overpotential for potential sweep Cu deposition by 0.6 V.[3] Present steady-state rotating disk measurements showed an increase of 75 mV (Figure 1). Cu corrosion is inhibited by an adsorbed layer of BTA in solutions containing less than 200 μM BTA.[2] Above 200 μM BTA Cu reduction is further inhibited by the formation of a thin film of cuprous-BTA on the deposit surface.[2] The addition of BTA to plating baths has been shown to reduce the crystal size of Cu deposits.[2] Benzotriazole has also been shown to alter the crystal habit of Cu films.[4] The crystal habit is related to the relative growth rates of the crystal faces.[5] The faces with the slowest growth rate dominate the surface of the crystal. The (210) facet dominates the surface of Cu electrodeposits from additive free electrolyte.[6]

In this study the effects of BTA on the nucleation density and the crystal habit were determined from the microtopography of Cu electrodeposits formed at several BTA concentrations and current densities.[7, 8]

STM Apparatus and Experimental Procedures

A Nanoscope I STM[9] with a 0.6 μm scanner was used in this investigation. The instrument was augmented by a PC-based data acquisition system which was interfaced with the microscope to digitally record STM images as a 200 x 320 point map of the probe height.[10] Platinum wires, cut with scissors, were used as the tunneling probes. Scanning electron micrographs of the tunneling probes showed, typically, a 300 nm radius of curvature at the tip, (Figure 2). Although very sharp tips could be made by this method about 70% of the tips had to be discarded due to the occurrence of multiple tunneling points (recognized as repetitive features in images). In an electrochemically active medium it is important to hold the probe potential in a region where no charge transfer reaction occurs.

The probe potential was therefore restricted by the potentials of Cu deposition and O_2 evolution in the electrolyte. An insulating coating of polyvinylidene fluoride on the tunneling probe was effective in reducing the magnitude of capacitive and charge transfer currents. The coating reduced the residual background current, (due to O_2 reduction) to less than 1 nA on Pt probes in the electrolyte (at a probe potential of 100 mV vs Cu). All STM measurements reported below were obtained with the constant current method in which the probe height is maintained to keep a constant probe current (1 to 5 nA) as the probe is rastered across the surface. The probe height follows the surface contour closely because the tunneling current is very sensitive to the probe-to-surface gap.

The electrochemical cell contained four electrodes: deposit substrate, counter electrode, reference electrode, and tunneling probe. The tunneling probe was held 30 mV anodic of the substrate by the Nanoscope I controller. The potential of the substrate relative to the reference electrode or the current between the substrate and the counter electrode was controlled by a PAR 173 potentiostat.[11] Electrical isolation of the potentiostat is necessary to prevent current loops between the potentiostat, STM controller, and ground. The potentiostat was connected to the 120 V_{AC} line with an isolation transformer and connected to ground through a 100 Ω resistor and 100 μF capacitor in series. Two configurations of the electrochemical cell were used. The first consisted of a Pt (111) substrate on which approximately 0.1 ml of electrolyte was held in a 3 mm high, 6 mm inside diameter polypropylene ring (welded to the substrate). Copper reference and counter electrodes were placed in separate external wells connected to the polypropylene ring with electrolyte-filled Teflon tubing. The second electrochemical cell consisted of a Pt (110) substrate on which approximately 0.1 ml of electrolyte was held by a 6 mm diameter Pt ring (made from 10 mil wire) located 1 mm from the substrate surface. The Pt ring also served as the counter electrode. A Cu reference electrode was inserted directly into the cell.

The nucleation density of Cu on Pt (110) was measured following galvanostatic deposition of 20 mC/cm^2 (7 nm compact film) of Cu. The composition of the electrolyte was 0.5 M $CuSO_4$ and 0.5 M H_2SO_4 with 0, 50, 100, or 200 μM BTA. The nucleation density was measured from deposits formed in the Pt ring electrochemical cell. The substrate was mechanically polished with 0.05 μm alumina and annealed in a natural gas flame. Prior to each deposition the substrate was cleaned by passing an anodic current of 1.6 A/cm^2 for approximately 4 s followed by a change in electrolyte. The copper deposit was made with a galvanostatic pulse. The tunneling probe was withdrawn from solution during the cathodic pulse to prevent shielding of the substrate by the tip. Following the pulse a constant current was applied to prevent deposit dissolution resulting from oxygen reduction. The level of this current was equal to the oxygen reduction current, determined from measurements on the Pt substrate at +2 mV vs Cu. Profiles of the nucleated deposit were taken; the deposit was then removed by electrochemical dissolution in order to determine the profile of the substrate. The nucleation density was estimated from a one dimensional fast Fourier transform (FFT) of the z height with respect to the scan direction. A FFT was determined for each scan line. The reported FFT is the average over the 320 scan lines of the STM raster scan.[7] The FFT interpretation was based on the assumption that the ratio of height to width of nuclei was constant. If the nuclei on the surface are touching and not overlapping, the characteristic frequency, f_s, of the profile is equal to the inverse of the width of the nuclei such that the product of the amplitude and frequency is constant irrespective of nucleation density. The characteristic frequency of the profile was experimentally determined from the peak value of the product of amplitude and frequency of a FFT of the surface (Figure 3). The nucleation density was estimated as $(f_s)^2$.

Sequential STM images of Cu were recorded during deposition at -25 mV following nucleation with a potentiostatic pulse to -500 mV relative to Cu. The composition of the electrolyte was 10 mM $Cu(ClO_4)_2$, 0.5 M $NaClO_4$, and 0.1 M $HClO_4$

with and without 10 μM BTA. The deposits were formed on a Pt (111) substrate which had been mechanically polished with 0.05 μm alumina, etched in warm *aqua regia*, and annealed for 12 hours at 1000 ^{o}C in vacuum. The polypropylene ring cell was used in the above measurements.

Bulk Cu deposits (> 1 μm) were formed on Pt (110) in 0.2 M $CuSO_4$, 0.5 M H_2SO_4, with 0 and 107 μM BTA. The Pt ring cell was used with a Cu wire reference electrode. The deposits were formed with the STM tip retracted from the surface. The substrate was mechanical polished with 0.05 μm alumina and annealed in a natural gas flame. The deposits were initiated with a 100 ms pulse to -500 mV to promote uniform nucleation. Following the pulse the potential was stepped to approximately -50 mV and the deposit was allowed to grow. Following the growth period the potential was stepped to -8 mV to avoid corrosion and the surface was imaged with STM.

Display of STM Topography

STM images are commonly displayed as either line scan plots of the height or grey scale plots of the height, tunneling current , or voltage.[12] These methods are well suited for displaying height information of comparable size but they do not adequately display images with a large range of height features because the line scan and grey scale plots of height are dominated by the large features in the scan area. When the important features are small relative to the overall topography, the height information is better represented by displaying the slope of the surface with a grey scale.[13] A relief image of the surface is obtained by assigning a grey scale to the local slope of the surface. The grey scale was spread between the most negative (dark) and positive (bright) values of the slope averaged over three points in the scan direction. This method of representing the STM data highlights small features since these features result in a rapid change in the slope of the

surface. In this study, the STM scans are represented by slope coded grey scale plots and height coded line scan plots. Line scan plots are used to quantitatively identify heights.

Nucleation Density

Figure 4 is the image of a Cu deposit formed in 100 μM BTA with a 200 ms 100 mA/cm^2 pulse. The underlying Pt substrate is completely covered with Cu particles with diameter less than 50 nm. The particles in Figure 4 appear spherical in shape, with an average diameter of 12 nm, and a nucleation density of 7.5×10^{11} $nuclei/cm^2$ (visually determined within the boundaries of a 0.029 μm^2 area in the center of the figure). Figure 3 shows the frequency dependence of the product of amplitude and frequency from Fourier transforms of the STM data of Figures 4 and 5. As based on the Fourier analysis, the surface imaged in Figure 4 has a spatial period of 32 nm corresponding to 9.8×10^{10} $nuclei/cm^2$. The Fourier interpretation results in a lower number density of nuclei because only one frequency (peak in Figure 3) is utilized. Direct counting includes nuclei of all sizes in the sampled area and not just those with the most common periodicity. The nucleation densities of the 20 mC/cm^2 Cu films reported in Figure 6 [7] were determined from Fourier transforms of the STM data. The nucleation densities show an upward trend with increasing overpotential with no significant difference between electrolytes containing 0, 50, 100, and 200 μM BTA. For comparison, Figure 5 shows the image of a typical substrate surface following dissolution of the copper deposit. The surface consisted of 10 nm wide terraces separated by 1 to 3 nm high steps.

STM of Growing Deposits

A thick deposit (>1μm) of Cu from BTA free electrolyte was formed with a 30 second pulse to -500 mV vs Cu with the tip removed from the surface. Following the

pulse the potential was stepped to -25 mV vs Cu at which time continuous scanning of the surface by the tunneling probe began. The deposit had long range order exceeding the width of the probe scan, 0.6 μm (Figure 7).[13] These deposits were faceted with deposition observed at steps. Short period roughness resulting from new nucleation is shown in the bottom right corner of Figure 7. Although rapid growth is observed in some areas of the electrode little change occurs in others, this can be seen by comparing the top and bottom portions of Figures 7a and 7b. Nonuniform deposition of copper is also seen for deposition on Cu free Pt at low overpotentials. At low overpotentials three dimensional growth centers of copper develop next to regions of bare Pt. Figures 8 and 9 are of a deposit grown in the absence of BTA at -50 mV. The deposit was faceted with planar surfaces extending over up to 200 nm. The facets are correlated across the width of the imaged area (600 nm). Figure 9 shows a peak to valley distance of approximately 35 nm.

The deposit from electrolyte containing 10 μM BTA was initiated with a 0.5 sec pulse to -500 mV vs Cu. The tip was at tunneling distance from the surface during the initial pulse. Following the 0.5 sec pulse the potential was stepped to -20 mV vs Cu. Before Cu deposition the bare Pt surface showed a stepped appearance with 2 nm ledges and atomically flat planes in between (Figure 10a). Following the initial pulse, deposition on the Pt planes resulted in a wavy surface with a period of approximately 20 nm and an amplitude of 0.5 nm (Figure 10b). This waviness is proposed to represent the island growth of the first two monolayers of deposit. Following further deposition, the development of larger oblong nuclei of approximately 2 nm height occurs (Figure 10c). Figures 11 and 12 are of a deposit grown in 107 μM BTA at -28 mV. The deposit consisted of hemispherical particles of less than 50 nm diameter.

Unlike the BTA-free deposit (Figure 7), the deposit from the BTA-containing electrolyte was not faceted and did not have long range order (Figure 10b, c). The propagation of ledges and the long range order of the deposit from a BTA-free electrolyte

indicates growth in preferred crystallographic directions. This preference is prevented by the action of BTA and uniform growth occurs. In the presence of BTA the Cu deposit develops from atomic height islands which coalesce into larger entities.

Conclusions

The sub-micron topography of electrodeposited copper in additive free electrolyte is governed by the preferential growth of a few crystallographic orientations. This anisoptropy of the kinetics of the different crystallographic directions results in insensitivity of the local growth rates, on the scale of the deposit particle, to interfacial concentration gradients of species affecting the deposition rate.

Electrodeposits from BTA containing electrolyte were free from faceting indicating uniform deposition kinetics in all crystallographic directions. The local deposition rate on the surface of a particle is governed by the concentration of species affecting the deposition rate. With kinetics that are independent of the crystallographic orientation, rapid brightening may occur in the presence of a second inhibitor that is depleted in the recesses of the surface.

The nucleation density of Cu on Pt depends on the applied potential, but is independent of the presence of BTA. The reduction of particle size of electrodeposits by the addition of BTA is the result of the higher overpotential required for deposition. The reduction of particle size is the primary reason for bright Cu plating in the presence of BTA.

Acknowledgement

This work was supported by the Director, Office of Energy Research, Office of Basic Energy Sciences Division, Materials Sciences Division of the U.S. Department of Energy under Contract No. DE-AC03-76SF00098.

1 O. Kardos and D.G. Foulke, in **Advances in Electrochemistry and Electrochemical Engineering**, Vol 2, C.W. Tobias Ed., Interscience, New York, 1962.

2 J.K. Prall and L.L. Shreir, *Corros. Sci.*, 1, 181 (1961).

3 Yu. M. Loshkarev, V. A. Omel'chenko, V. F. Vargalyuk, V. V. Trofimenko, L. P. Snetkova, and A. A. Rysakov, *Elektrokhimiya*, 10, 723 (1974).

4 B.S. Sheshadri and T.H.V. Setty, *Indian Journal of Chemistry*, 2, 927 (1973).

5 J.W. Mulin, in **Crystal Growth**, B.R. Pamplin Ed., Pergamon Press, New York, 1975, p 300.

6 U. Bertocci and D.R. Turner, in **Encyclopedia of Electrochemistry of the Elements,** A. J. Bard Ed., Vol. 2, p 384, Marcel Dekker Inc., New York (1974).

7 M.J. Armstrong and R.H. Muller, Electrochem. Soc. Meeting, Seattle, Oct. 14-19, 1990.

8 M.J. Armstrong and R.H. Muller, "The Role of Inhibitors During Electrodeposition of Thin Metallic Films", Ph. D. Thesis, Univ. of Calif., Berkeley, 1990.

9 Digital Instruments Inc., Goleta, California, 93117, USA.

10 M. J. Armstrong and R. H. Muller, *J. Electrochem. Soc.*, 136, 584 (1989).

11 Princeton Applied Research Corp., Princeton, New Jersey, 08540, USA.

12 P. K. Hansma and J. Tersoff, *J. Appl. Phys.*, 61, R1 (1987)

13 M.J. Armstrong and R.H. Muller, Electrochem. Soc. Meeting, Los Angeles, May 7-12 1989, ext. abstr. No. 525.

Figure Captions

Figure 1. Tafel plot of the potential-current relationship for Cu deposition from 0.5 M H_2SO_4, 0.5 M $CuSO_4$, with 0, 100, and 200 μM BTA. Rotating disk, 700 rpm. Potential corrected for a 2.3 Ω ohmic drop through the cell. (XBL 902-610)

Figure 2. Scanning electron micrograph of the tip of an STM probe (10 mil Pt wire cut with scissors). (XBB 906-5081)

Figure 3. FFT of the probe height with respect to the distance in the scan direction of a (□) 20 mC/cm^2 Cu deposit and the (o) underlying Pt substrate. Cu deposit formed by a 100 mA/cm^2 pulse in 0.5 M $CuSO_4$, 0.5 M H_2SO_4, with 100 μM BTA. FFT of the deposit contour indicates periodicity of nuclei of 32 nm (9.8×10^{10} nuclei/cm^2). (XBL 906–2302)

Figure 4. STM image of a 20 mC/cm^2 Cu deposit on a Pt substrate (shown in Figure 5); displayed with a derivative-coded grey scale. Deposit formed by a 100 mA/cm^2 pulse in 0.5 M $CuSO_4$, 0.5 M H_2SO_4, with 100 μM BTA. FFT of the deposit contour indicates periodicity of nuclei of 32 nm (9.8×10^{10} nuclei/cm^2). (XBB 901-554)

Figure 5. STM image of flame-annealed Pt substrate; displayed with a derivative-coded grey scale. The surface consisted of 10 nm wide terraces separated by 1 to 3 nm high steps. There are also a small number of protrusions on the surface. (XBB 901-555)

Figure 6. Effect of overpotential and BTA concentration on the number densities of nuclei of 20 mC/cm^2 Cu desposits on Pt. Number densities of nuclei derived from FFT of the deposits. Cu deposits formed from 0.5 M $CuSO_4$, 0.5 M H_2SO_4, with (□) 0, (o) 50, (+) 100, and (x) 200 μM BTA. (XBL 906-2301)

Figure 7. STM images of a Cu deposit formed by a 30 s pulse to - 500 mV followed by a step to -25 mV vs Cu in BTA-free 10 mM $Cu(ClO_4)_2$, 0.5 M $NaClO_4$, 0.1 M $HClO_4$ electrolyte; displayed with a derivative-coded grey scale. a) initial deposit and b) following 30 seconds at -25 mV vs Cu. Propagation of crystal facets (2 nm height) from lower left corner of a) to center of b). (XBB 880-11214A)

Figure 8. STM image of a Cu deposit grown in BTA-free 0.5 M H_2SO_4, 0.5 $CuSO_4$ at –50 mV; displayed with a derivative-coded grey scale. Faceted deposit with planar surfaces extending over up to 200 nm. (XBB 902-1427)

Figure 9. STM line scan plot of a Cu deposit grown in BTA-free 0.5 M H_2SO_4, 0.5 $CuSO_4$ at -50 mV shown in Figure 8. Peak-to-valley distance of approximately 35 nm. (XBL 907-6431)

Figure 10. STM images of a Cu deposit formed by a 0.5 s pulse to -500 mV followed by a step to -25 mV vs Cu in 10 mM $Cu(ClO_4)_2$, 0.5 M $NaClO_4$, 0.1 M $HClO_4$ with 10 μM BTA; displayed with a derivative-coded grey scale. (a) Pt substrate, (b) 30 s after pulse, and (c) 90 s after pulse. Formation of 20 nm diameter islands of 0.5 nm height (b) and growth to 2 nm height (c). (XBB 880-11212A)

Figure 11. STM image of a Cu deposit grown in 0.5 M H_2SO_4, 0.5 $CuSO_4$ with 107 μM BTA at -28 mV; displayed with a derivative-coded grey scale. Hemispherical particles of less than 50 nm diameter. (XBB 894-3042)

Figure 12. STM line scan plot of a Cu deposit grown in 0.5 M H_2SO_4, 0.5 $CuSO_4$ with 107 μM BTA at -28 mV shown in Figure 11. (XBL 907-6430)

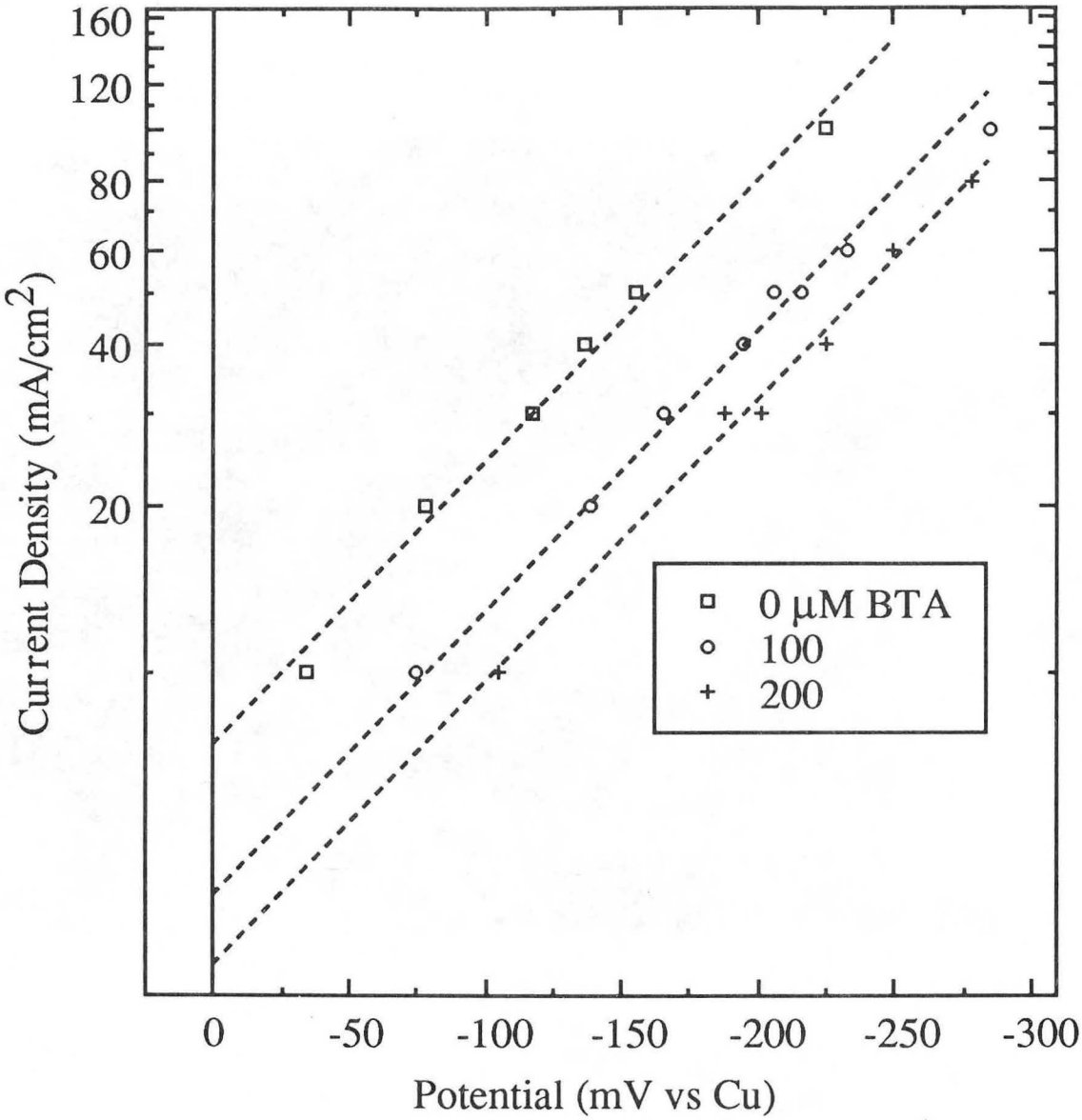

XBL 902-610

Fig. 1

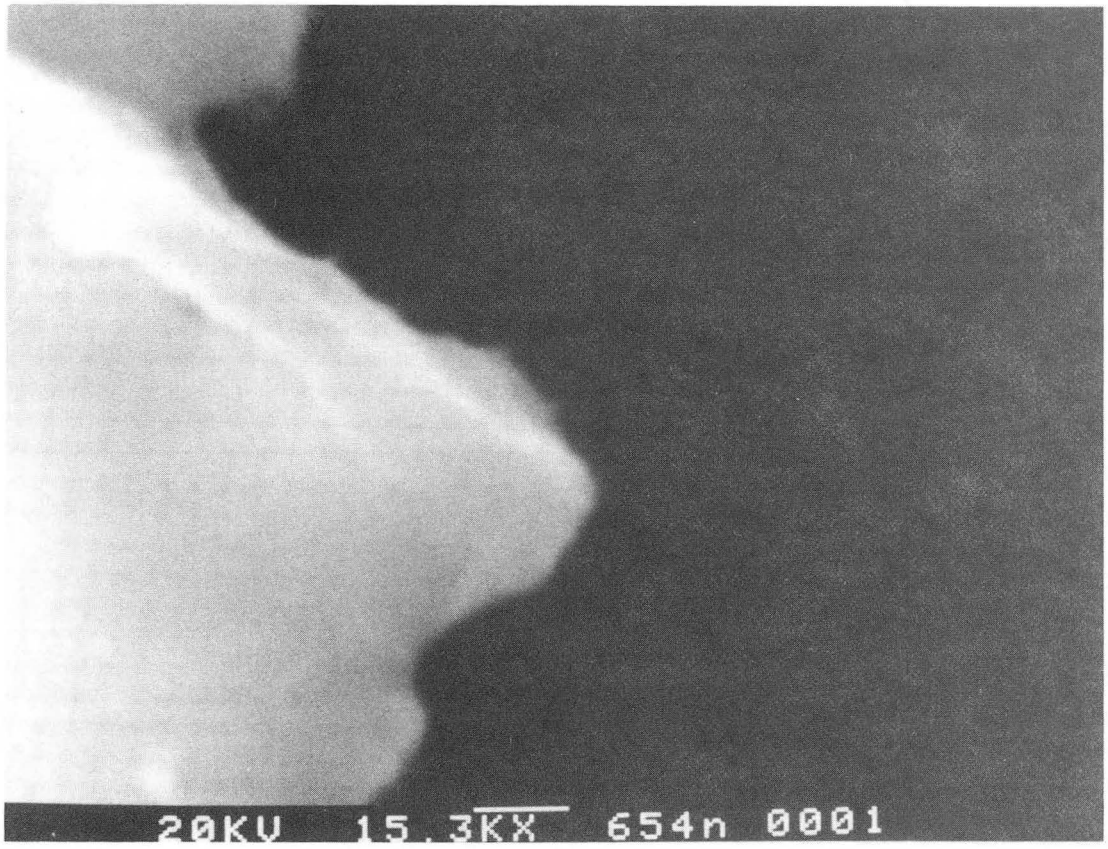

XBB 906-5081

Fig. 2

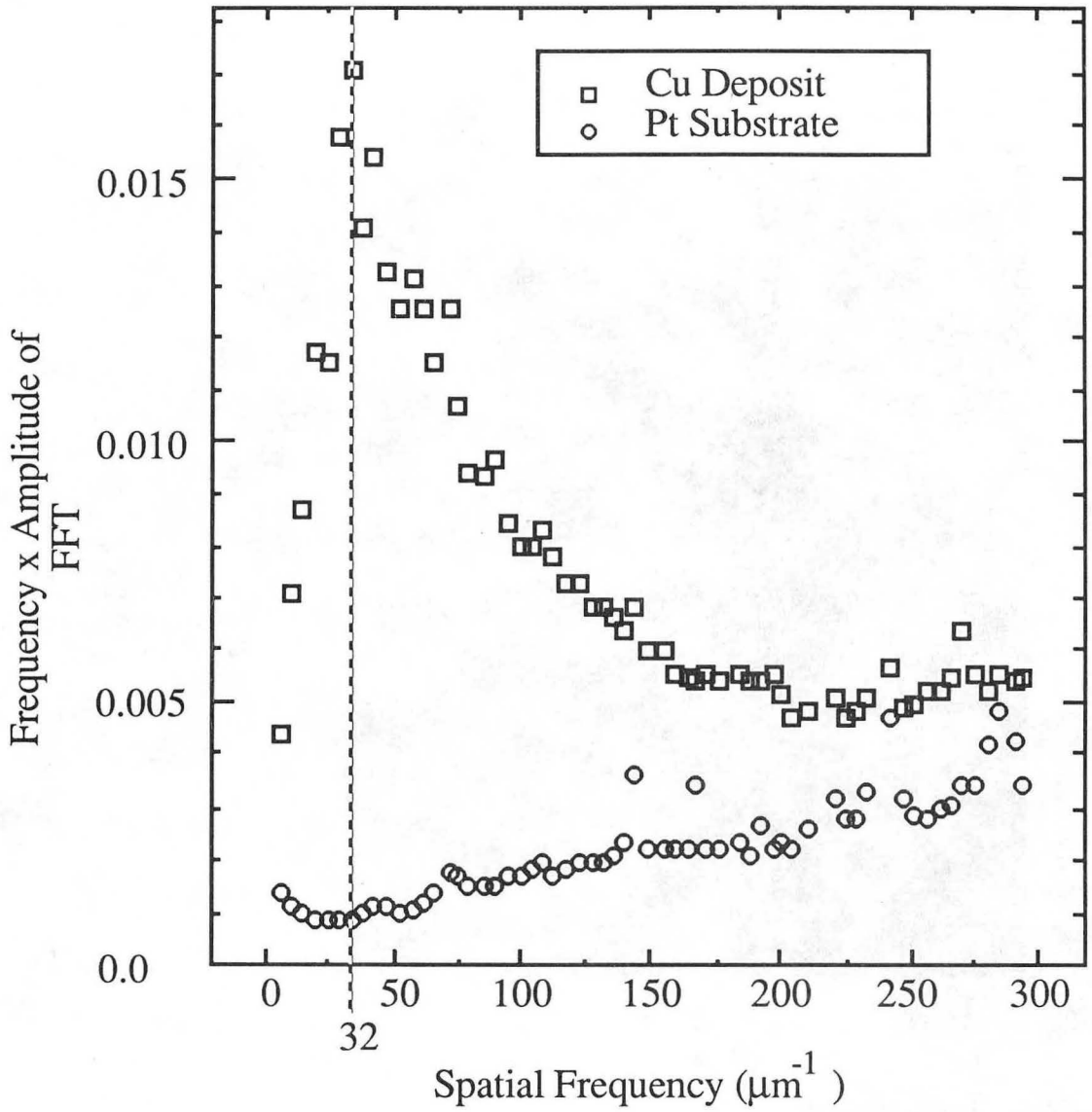

XBL 906-2302

Fig. 3

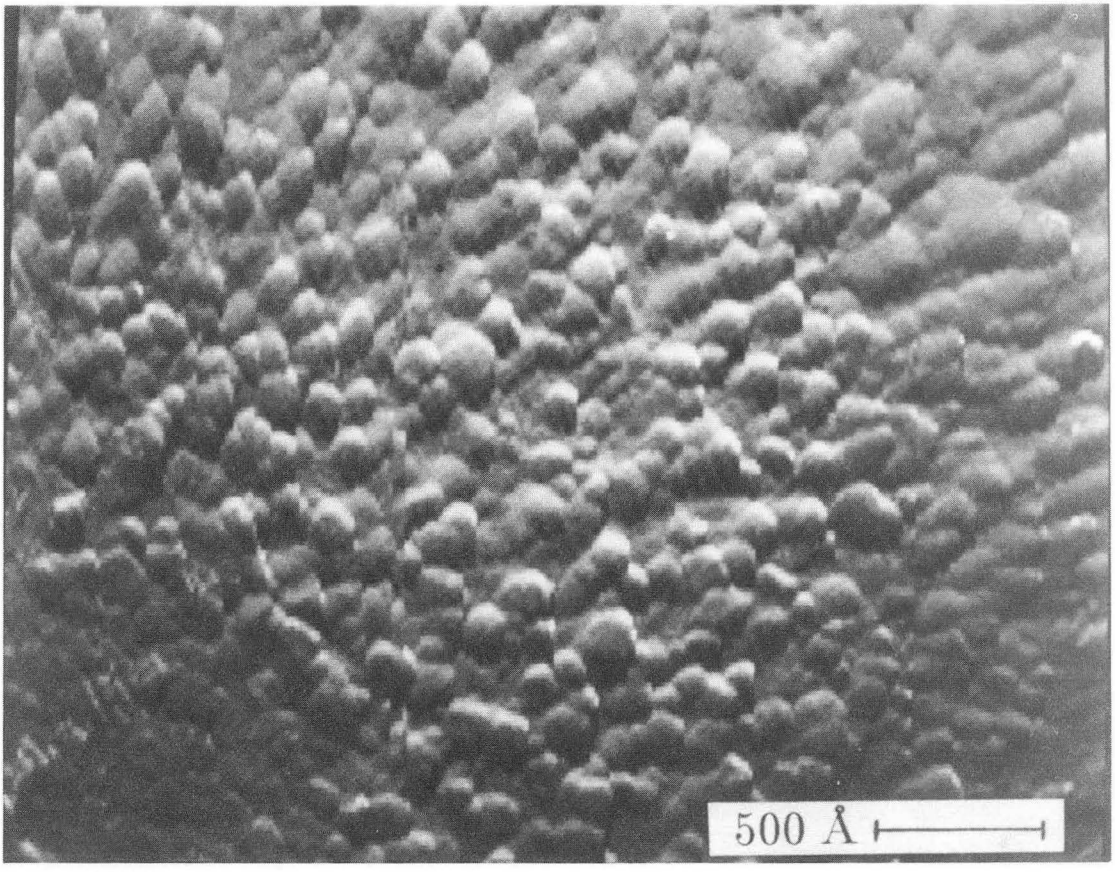

XBB 901-554

Fig. 4

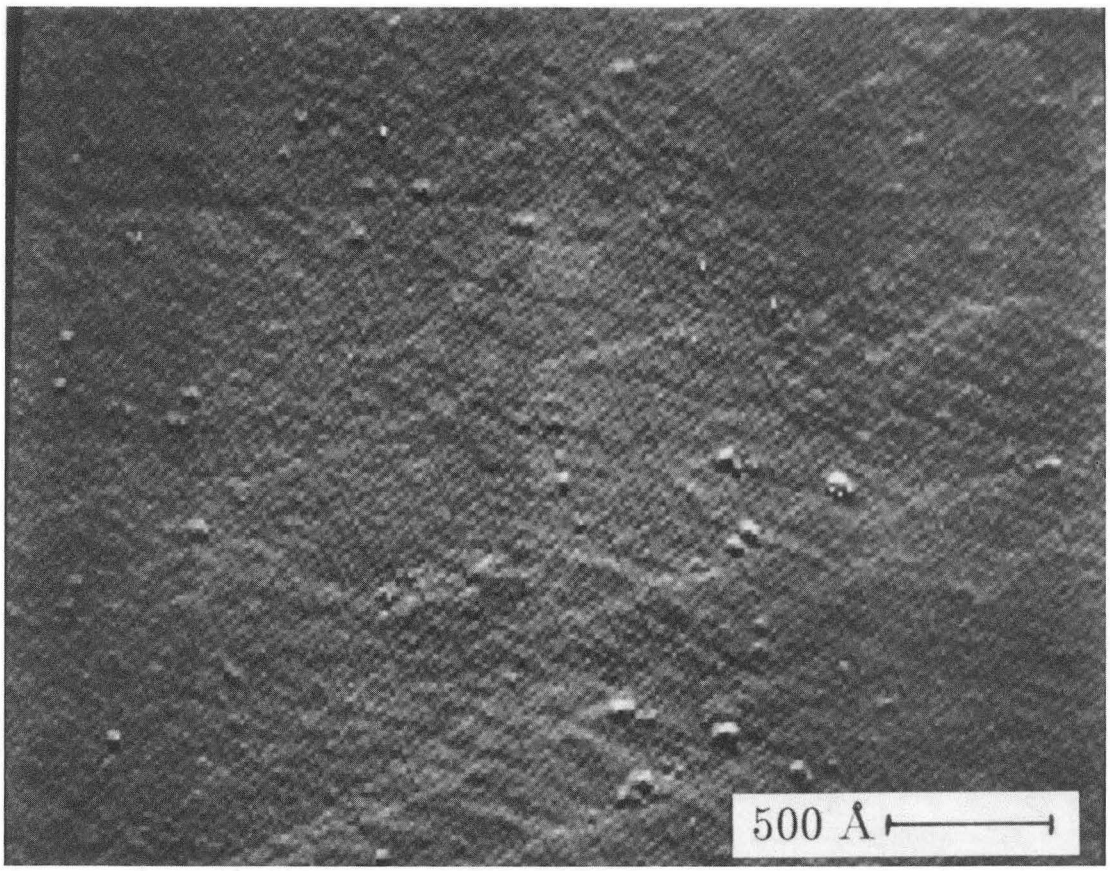

XBB 901-555

Fig. 5

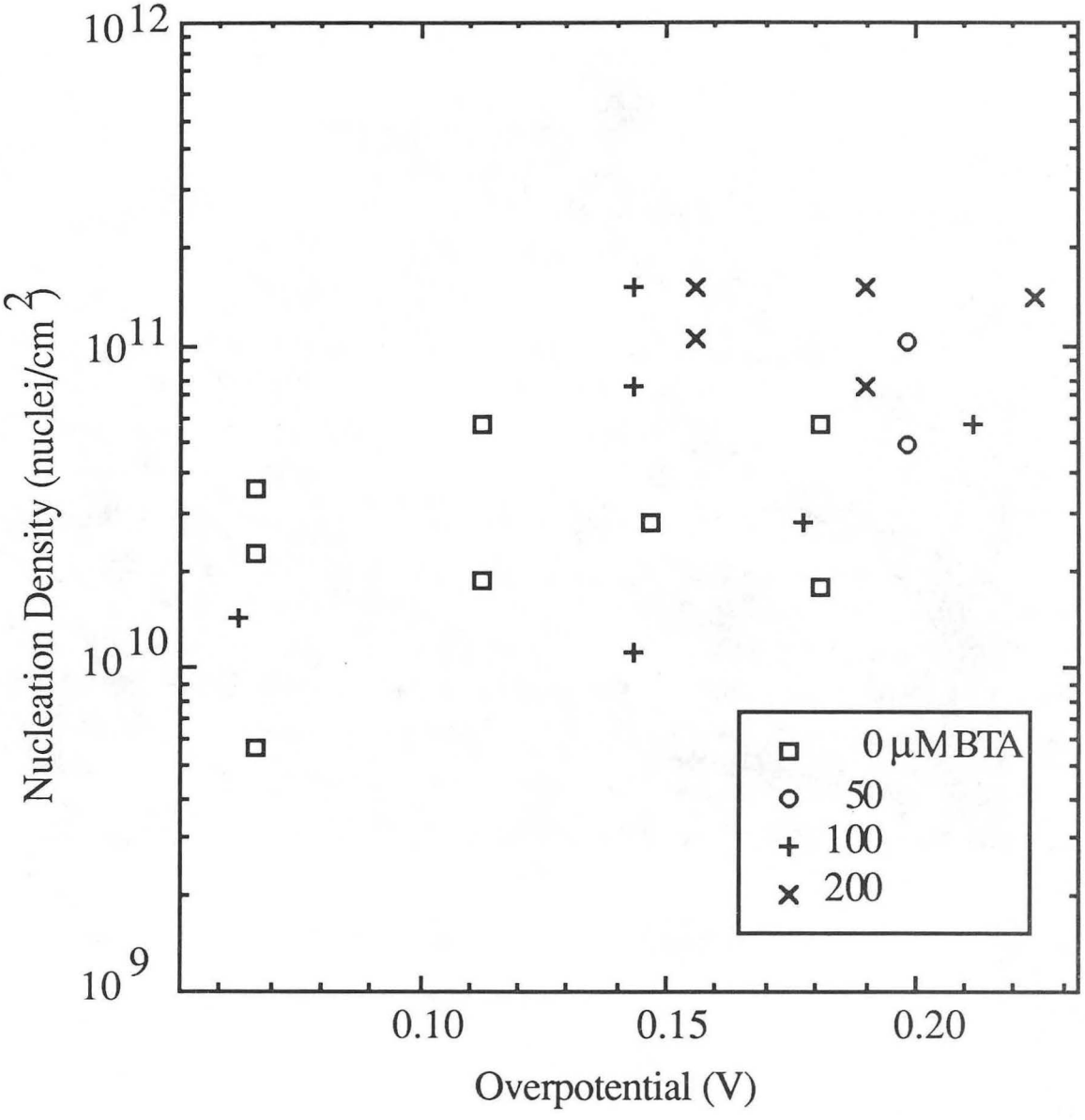

XBL 906-2301

Fig. 6

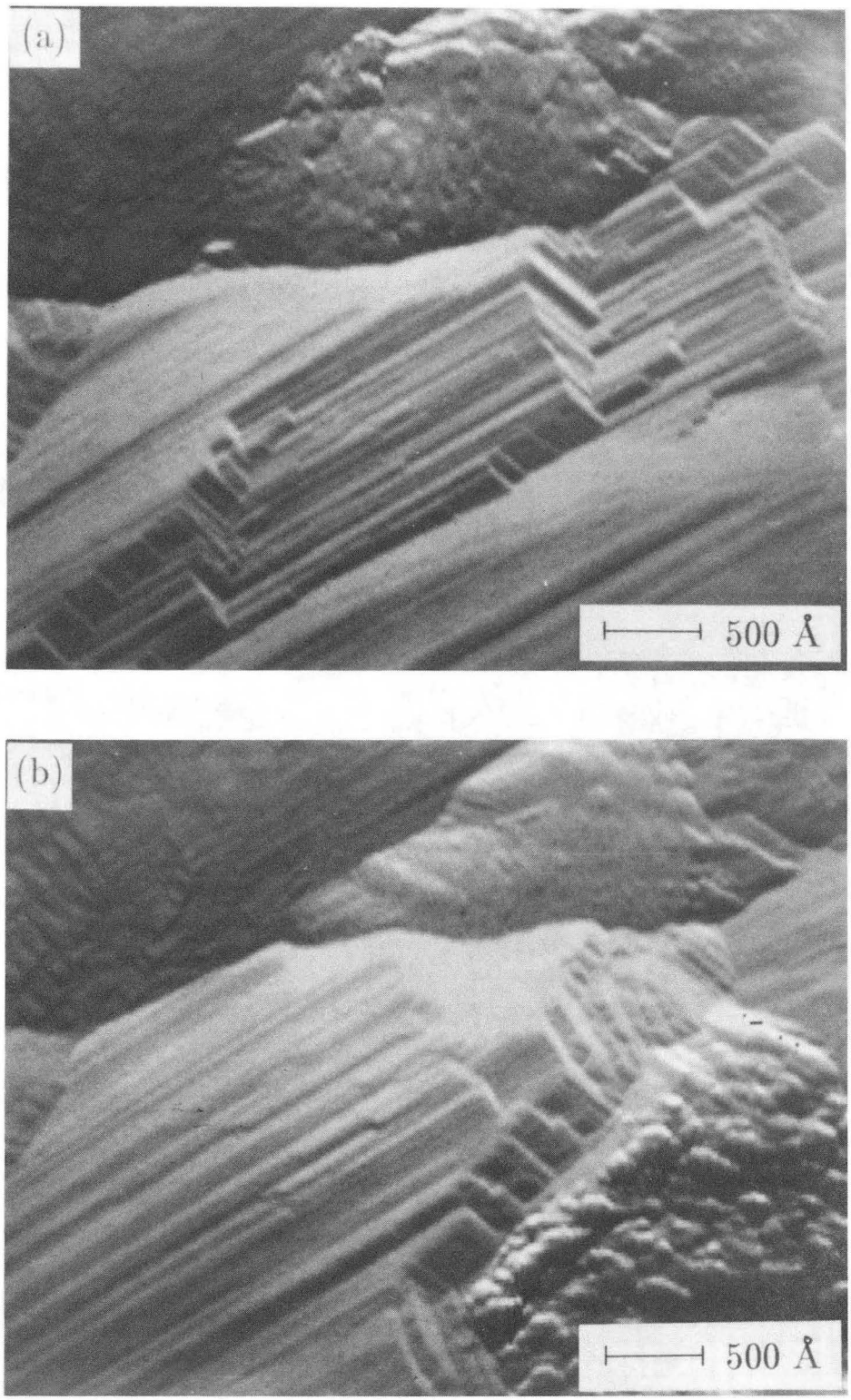

XBB 880-11214A

Fig. 7

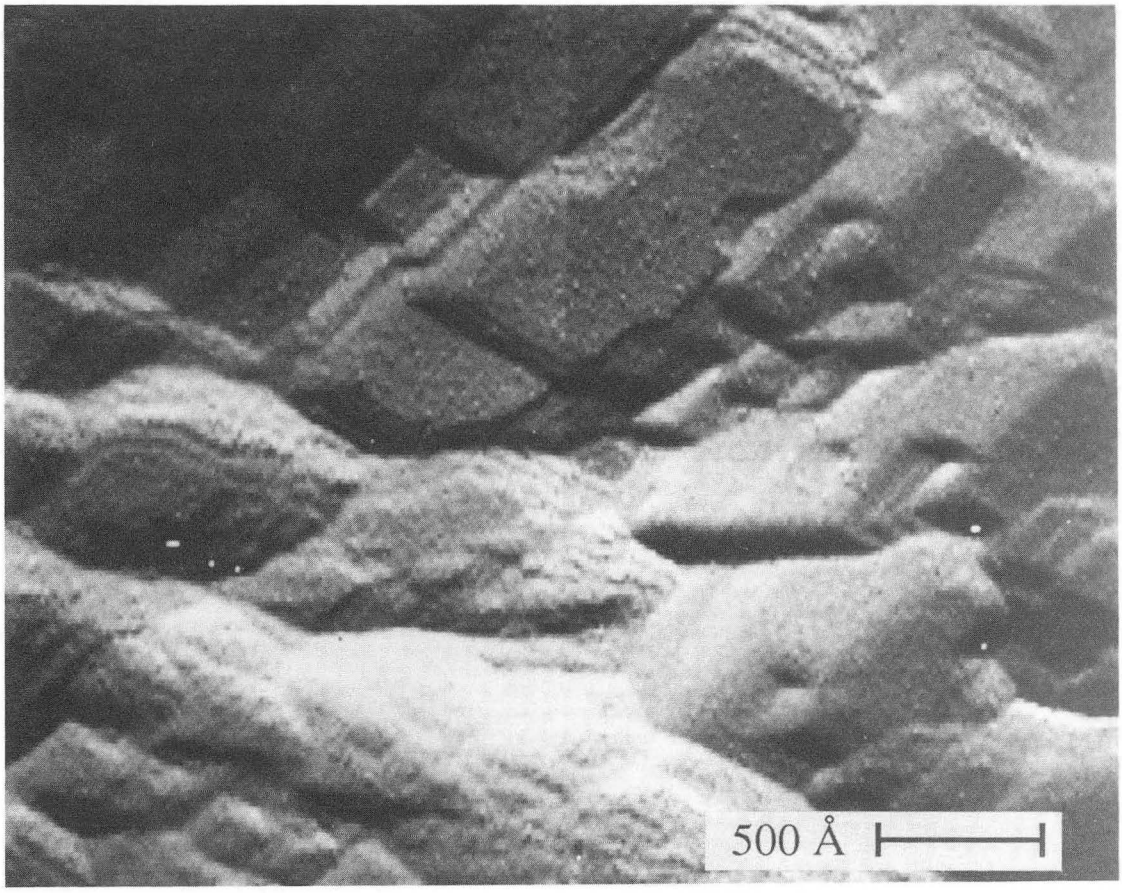

XBB 902-1427

Fig. 8

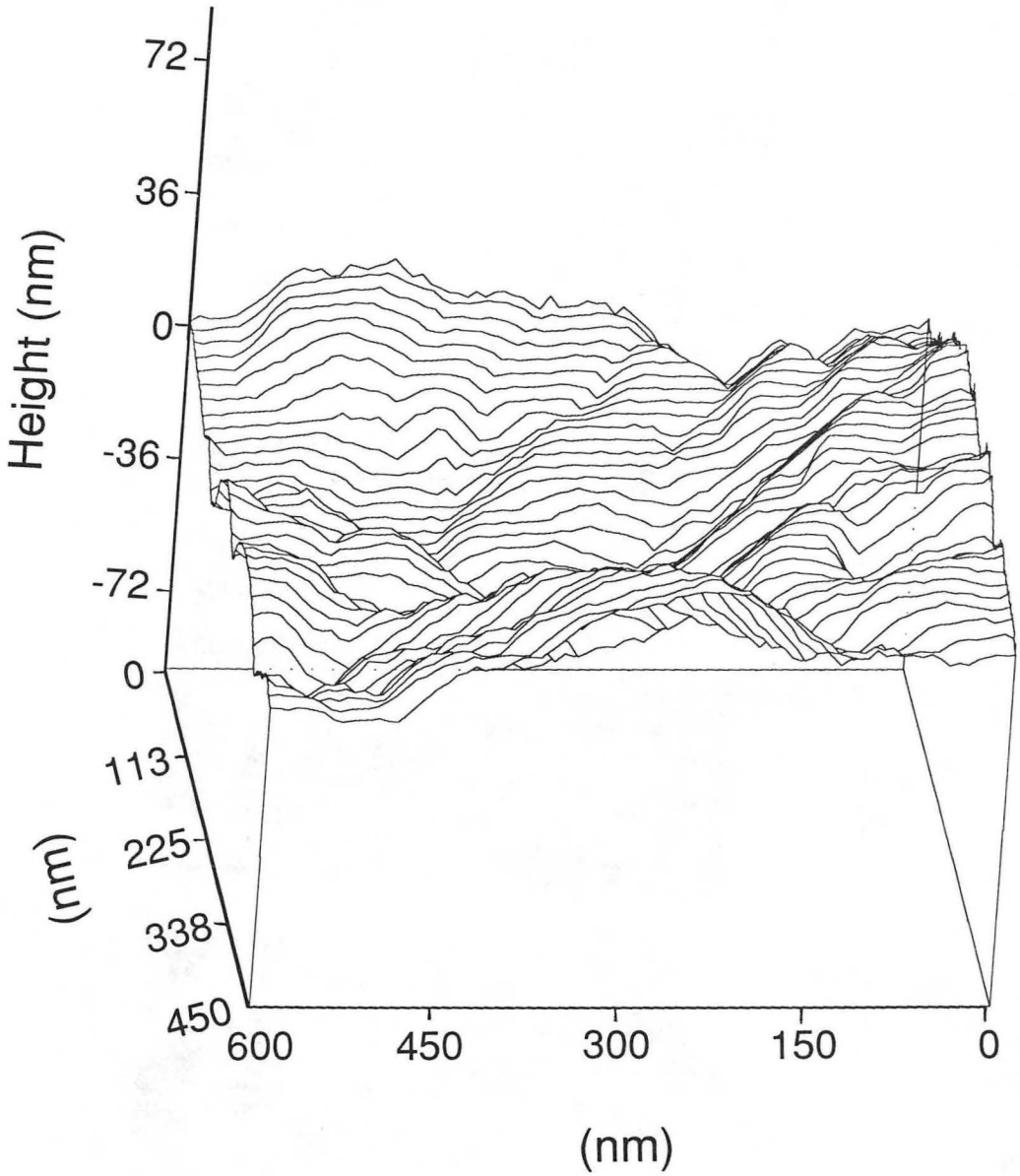

XBL 907 – 6431

Fig. 9

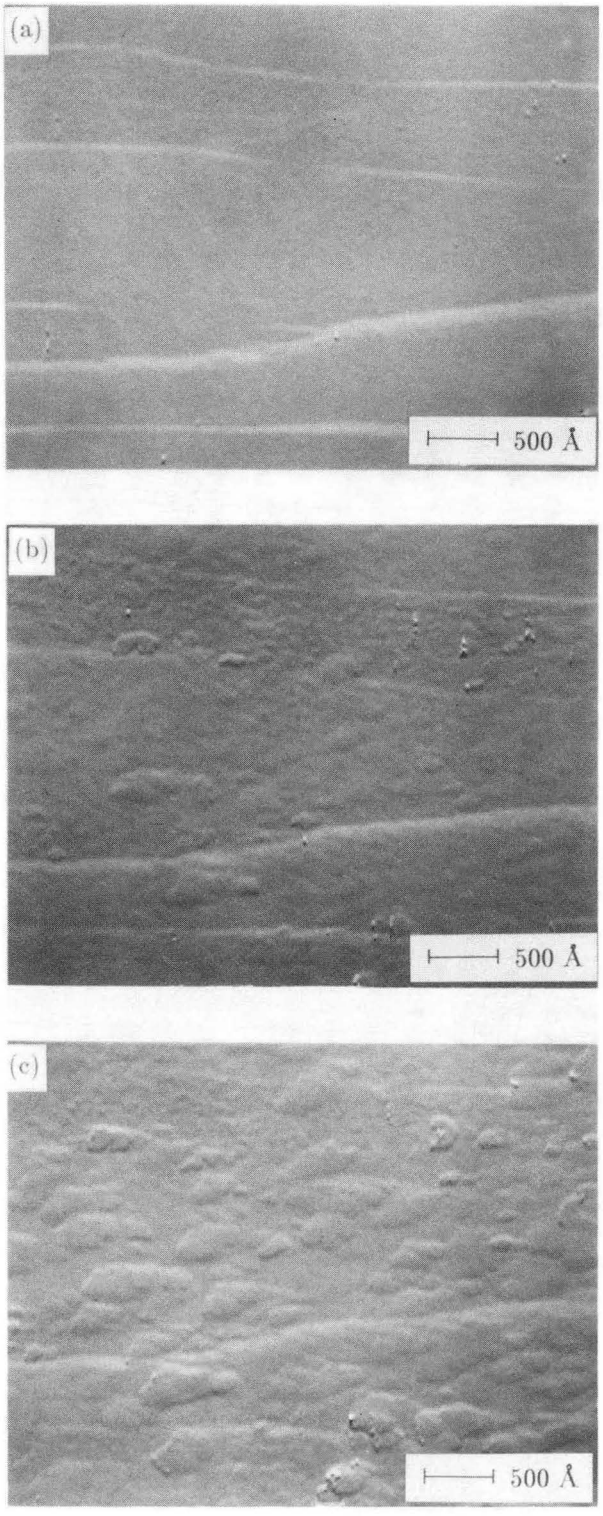

XBB 880-11212A

Fig. 10

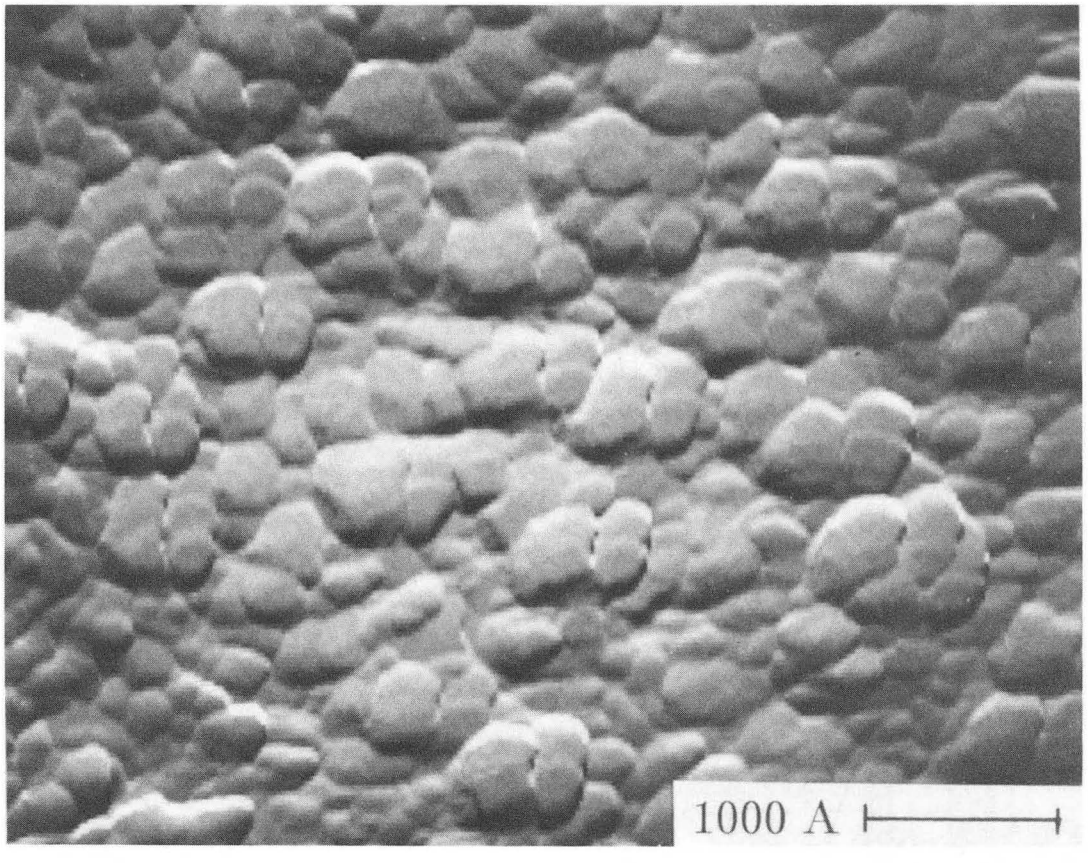

XBB 894-6430

Fig. 11

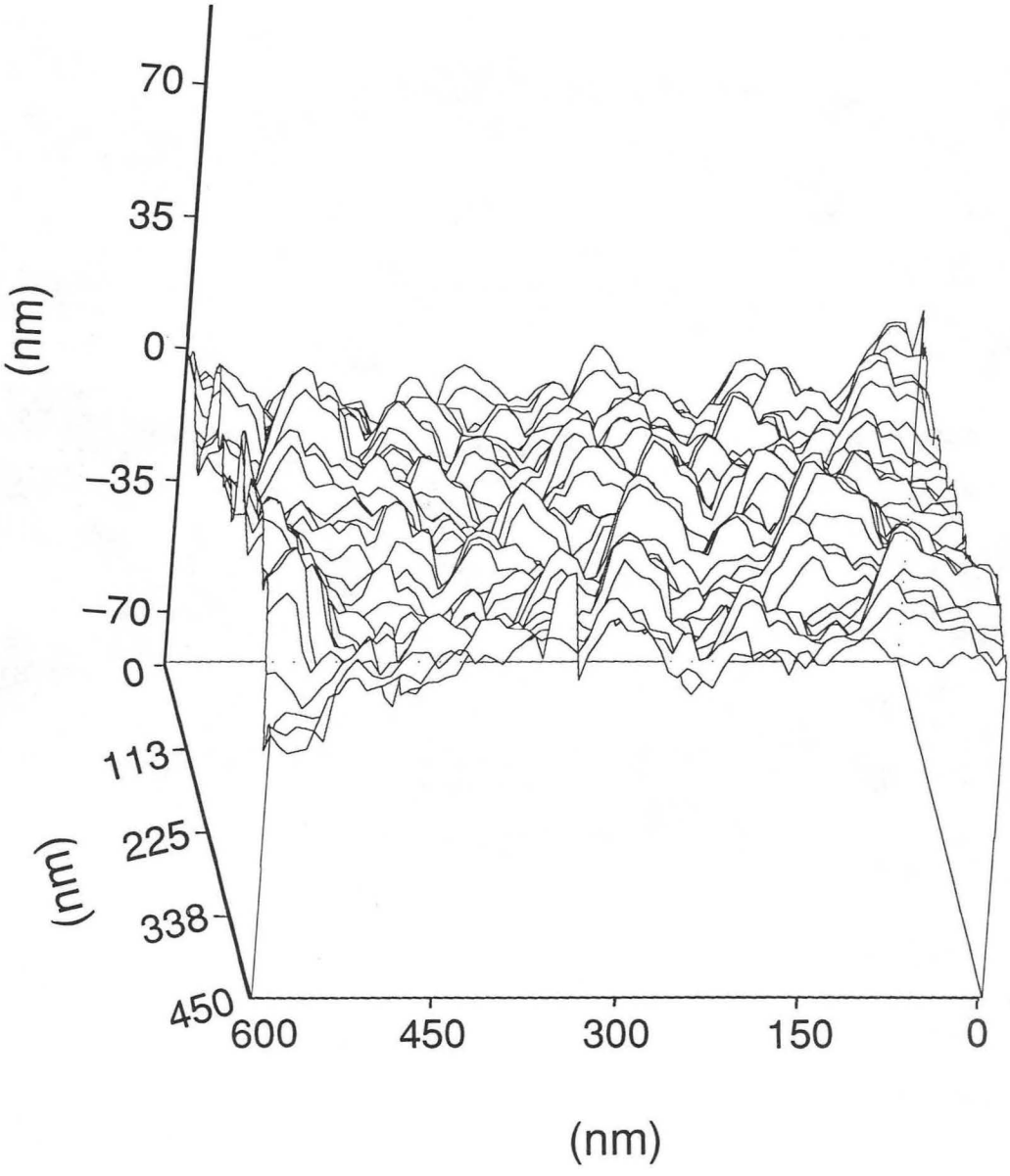

XBL 907 –6430

Fig. 12

LAWRENCE BERKELEY LABORATORY
UNIVERSITY OF CALIFORNIA
INFORMATION RESOURCES DEPARTMENT
BERKELEY, CALIFORNIA 94720